

NJC

Accepted Manuscript



This is an *Accepted Manuscript*, which has been through the Royal Society of Chemistry peer review process and has been accepted for publication.

Accepted Manuscripts are published online shortly after acceptance, before technical editing, formatting and proof reading. Using this free service, authors can make their results available to the community, in citable form, before we publish the edited article. We will replace this *Accepted Manuscript* with the edited and formatted *Advance Article* as soon as it is available.

You can find more information about *Accepted Manuscripts* in the [Information for Authors](#).

Please note that technical editing may introduce minor changes to the text and/or graphics, which may alter content. The journal's standard [Terms & Conditions](#) and the [Ethical guidelines](#) still apply. In no event shall the Royal Society of Chemistry be held responsible for any errors or omissions in this *Accepted Manuscript* or any consequences arising from the use of any information it contains.

Cite this: DOI: 10.1039/c0xx00000x

www.rsc.org/njc

PAPER

Color Tuning in Thermally Stable Sm³⁺-Activated CaWO₄ Nanophosphors

Maheshwary^a, B. P. Singh^b and R. A. Singh^{a*}

Received (in XXX, XXX) Xth XXXXXXXXX 20XX, Accepted Xth XXXXXXXXX 20XX

DOI: 10.1039/b000000x

Abstract:

This paper reports CaWO₄:Sm³⁺ nanophosphors with varying compositions of Sm³⁺ (Sm³⁺ = 2, 5, 7 and 10 at.%). As-prepared (ASP) samples were annealed at 800 °C for 2 h to eliminate unwanted organic moieties present in the sample and to improve crystallinity. These nanoparticles are characterized employing X-ray diffraction (XRD), differential thermal analysis (DTA), thermogravimetric (TG) analysis, Fourier-transform IR spectroscopy (FT-IR), Transmission electron microscopy (TEM), X-ray photoelectron spectroscopy (XPS), UV-vis spectroscopy, Raman spectroscopy, photoluminescence studies and lifetime decay studies. The as-prepared samples exhibit a spherical morphology having particle size of ~ 18-25 nm. TG study reveals that the nanophosphors are thermally stable. Excitation spectra corroborate that these were efficiently excited over a broad wavelength range (250-405 nm). As-prepared and 800 °C annealed samples of CaWO₄:Sm³⁺ (Sm³⁺ = 2, 5, 7 and 10 at.%) nanoparticles show blue and green luminescence because of strong host contribution, and warm white luminescence because of different energy transfer rates from host to Sm³⁺ ions under 250 and 405 nm excitations, respectively. This color tunability is also verified by CIE diagram. The critical distances R_c were found to be ~ 19.58 and 19.62 Å for ASP and 800 °C annealed 2 at.% Sm³⁺-doped CaWO₄, respectively. Using Van Uitert's model the type of interaction between Sm³⁺ ions was confirmed as the dipole-dipole interaction. The CCT (Color Correlated Temperature) values under 405 nm are in the range ~1950-2900 K. These studies reveal that the emission colors can be effectively tuned by altering the excitation wavelength and annealing temperature, and these materials may be potential candidates for white light emitting diodes.

KEYWORDS: Energy Transfer, Host Sensitization, Thermal Stability, CIE, CCT, Lifetime.

1. Introduction

In recent years, white light based light emitting diodes have attracted significant attention due to their superiority over conventional incandescent and fluorescent light sources. wLEDs have long operating lifetime, higher luminous efficiency, reliability and higher energy efficiency.^{1,2} The present strategy to produce white light utilizes combination of blue LED with yellow luminescence from Y₃Al₅O₁₂:Ce³⁺ (YAG:Ce) phosphor materials. However, it has some demerits such as narrow visible range, poor color rendition; thermal quenching and color degradation at high temperature generated during LED operation.³ Thus, it is required to develop a phosphor which has high quantum efficiency and ability to withstand high temperatures generated during the LED action without compromising the luminescence.

Recently, tungstates compounds have emerged as an important

family of luminescent materials because of excellent thermal stability, interesting luminescence behavior, self-activated nature, good thermal stability, wide emission spectra in visible region and attractive structural properties.^{4(a)-(h)} They found their applications in optical fibers, laser host materials, photoluminescence, scintillation detectors and microwave application.⁵⁻⁷ Among tungstates, CaWO₄ is an efficient host material due to its opto-electrical properties based on its blue luminescence at room temperature.^{4(a),(d),8} CaWO₄ has scheelite type tetragonal structure having space group I4₁/a(88), in which W ions are isolated from each other and trapped between tetrahedral O-ion cages while the Ca ion is surrounded by eight oxygen ions.⁹ The luminescence properties of CaWO₄ can be enhanced by doping various rare-earth ions which results in broad and intense absorption bands. Several papers on the luminescent properties of CaWO₄ doped with rare earth ions have been published.^{8,10,11} However, there are no reports on the efficient

phosphors with thermally stable blue emissions for white light LEDs based on CaWO_4 host matrix. It is well known that Sm^{3+} acts as an activator in a variety of hosts such as rare earth oxides, silicates, tungstates, molybdates and phosphates.^{12(a)-(d)} Sm^{3+} -doped host lattices have found their frequent application as red phosphors.¹³⁻¹⁷ Former workers have studied the effect of Sm^{3+} ions concentration on the luminescence intensity of various host lattices.¹⁸⁻²⁰ However, no single-phosphor, single-emitting-center-converted white light-emitting diodes can simultaneously satisfy the color temperature and rendition requirements due to the lack of sufficient red spectral component in the phosphor's emission spectrum.

In this regard, synthesis and photoluminescence properties of thermally stable Sm^{3+} -activated CaWO_4 phosphors have been reported for white light-emitting diodes. Substantial approaches have been employed to synthesize CaWO_4 and/or CaWO_4 doped with Ln^{3+} with regular particle size and morphological control such as combustion process⁸, solid state reactions^{21,22}, Czochralski technique²³, hydrothermal method^{24,25}, co-precipitation process²⁶ and solvothermal route²⁷.

However, these chemical routes are not able to produce pure crystalline materials at low temperature. Herein, we have synthesized CaWO_4 doped Sm^{3+} ion ($\text{Sm}^{3+} = 2, 5, 7$ and 10 at.%) nanophosphors using polyol method under urea hydrolysis at low temperature (~ 150 °C) using ethylene glycol as reaction medium as well as capping agent and their luminescent properties have been investigated in detail as varying concentration of Sm^{3+} ion. The thermal stability of $\text{CaWO}_4:\text{Sm}^{3+}$ was found to be better than commercially available YAG:Ce phosphor at temperatures higher than 300 °C. The emission spectrum of $\text{CaWO}_4:\text{Sm}^{3+}$ shows that the most intense peak is located at 644 nm, which corresponds to the electric dipole ${}^4\text{G}_{5/2} \rightarrow {}^6\text{H}_{9/2}$ transition of Sm^{3+} in Ca sites without inversion symmetry. Critical distance R_c between Sm^{3+} - Sm^{3+} calculated by concentration quenching method is 19.6 Å. The decay curves of Sm^{3+} emission were measured to understand the mechanism behind the energy transfer processes. Color-tunable emission in $\text{CaWO}_4:\text{Sm}^{3+}$ phosphors can be obtained by the modulation of excitation wavelength, annealing temperature and the concentration of Sm^{3+} ions. Also, phosphor-converted white light-emitting diodes for indoor illumination need to be warm-white (i.e., correlated color temperature (CCT) < 4000 K) with good color rendition (i.e., color rendering index > 80).²⁸ Here, under 250 nm excitation $\text{CaWO}_4:\text{Sm}^{3+}$ ($\text{Sm}^{3+} = 2, 5, 7$ and 10 at.%) nanoparticles show blue and green luminescence because of strong host contribution, whereas under 405 nm excitation samples show warm white luminescence, because of different energy transfer rates from host to Sm^{3+} . The correlated color temperature obtained for the as-prepared and 800 °C annealed phosphors under 405 nm excitation ranges from ~ 1900 – 3000 K (warm white light). Thus, a series of emission tunable phosphors from green to bluish white and to orange-red emission colors were obtained by controlling the Sm^{3+} ion concentration and by adjusting the excitation wavelength. To the best of our knowledge, Sm^{3+} -doped CaWO_4 nanophosphors emitting in blue, green and red region have not been reported till now. These studies suggest that the reported phosphors can be used as a potential single-emitting-center-converted in white light-emitting diodes.

2. Experimental Details

2.1 Material Synthesis

CaWO_4 doped with Sm^{3+} ($\text{Sm}^{3+} = 2, 5, 7$ and 10 at.%) nanophosphors were prepared using ethylene glycol (EG) as both capping agent and reaction medium at 150 °C. The starting materials used were calcium chloride (CaCl_2 , AR), samarium oxide (Sm_2O_3 , 99.99%, Sigma Aldrich) and sodium tungstate dihydrate ($\text{Na}_2\text{WO}_4 \cdot 2\text{H}_2\text{O}$, AR). In a typical synthesis procedure of 5 at.% Sm^{3+} -doped CaWO_4 nanoparticles, 0.019 g of Sm_2O_3 was dissolved in concentrated nitric acid (HNO_3) to form $\text{Sm}(\text{NO}_3)_3$. The mixture was heated at 80 °C to remove the excess of acid and the process of removal of excess of acid was repeated five times after addition of deionized water (5 ml). After that 0.237 g of CaCl_2 and 0.743 g of $\text{Na}_2\text{WO}_4 \cdot 2\text{H}_2\text{O}$ were dissolved in distilled water and CaCl_2 solution was mixed with $\text{Sm}(\text{NO}_3)_3$ and 25 ml of EG was then added to both the solutions. The pH of the solution was adjusted to $9-9.5$. The mixed solutions were dropped into Na_2WO_4 solution under constant stirring. This solution is then transferred to a two neck round bottom flask and was heated upto 150 °C for 3 hours under refluxing condition in a condenser until precipitation was complete.

The white precipitate so obtained was washed 3 times in methanol to remove excess of EG and finally it was washed with acetone and dried at 90 °C for 2 hours in vacuum oven to yield the final white product. CaWO_4 phosphors doped with $2, 7$ and 10 atomic percentages (at.%) of Sm^{3+} were synthesized by the same procedure.

The obtained white precipitate was divided in 2 parts. One part of the sample was annealed at 800 °C in an ambient atmosphere at a heating rate of 2 °C min^{-1} for 2 hours in an alumina crucible and the other part was left untreated.

2.2 Characterization

To identify the phase structure, X-ray diffraction (XRD) analysis was done with a Bruker D8 Advance X-ray diffractometer (Cu $\text{K}\alpha$ 1 irradiation, $\lambda = 1.5406$ Å) radiation at 40 KV and 40 mA at $4^\circ(2\theta)/\text{min}$ scanning rate. All patterns were recorded over the angular range $10^\circ \leq 2\theta \leq 80^\circ$ with a step size of $\Delta 2\theta = 0.02$. The surface morphology and particle size of the nano-particles were characterized by Transmission Electron Microscopy (TEM) using a Tecnai G^2 20 operated at an acceleration voltage of 200 kV. For TEM measurement, the samples were dispersed in methanol. A drop of the dispersed particles was put over the carbon coated copper grid and dried in the ambient atmosphere. Simultaneous DSC/TGA spectra were recorded using NETZSCH STA 449 F1. DSC and TG analyses were carried out using 10 mg of the sample at a heating rate of 10 °C min^{-1} up to 1000 °C, in nitrogen atmosphere under a flow of 60 $\text{cm}^3 \text{min}^{-1}$. Infrared spectra were recorded on a Fourier transform infrared (FT-IR) spectrophotometer (Shimadzu model 8400 S) with a resolution of 2 cm^{-1} and in the range $400-4000$ cm^{-1} . For IR measurement the samples were mixed with KBr (Sigma Aldrich, 99.99 %) in $1:5$ ratio and this mixture was placed in a sample holder and the spectra were recorded. The chemical binding energies of the respective ions in the sample were measured using X-ray photoelectron spectroscopy (XPS) SPECS, Germany (Mg $\text{K}\alpha$ X-ray source, $h\nu = 1253.6$ eV). UV-vis spectra were recorded using

UV-2700 Double beam spectrophotometer in the reflection mode. Raman spectra of the as-prepared and annealed samples were measured with Renishaw micro-Raman spectrometer attached with 633 nm laser as an excitation source.

The photoluminescence (PL) and photoluminescence excitation (PLE) spectra of the samples were recorded. Lifetime decay was recorded with Edinburg instrument F-920 equipped with 100 W μ s flash xenon lamp as the excitation source.

3. Results and discussion

3.1 XRD Study

The XRD patterns of as-prepared and 800 °C annealed Sm^{3+} (2, 5, 7 and 10 at.%) doped CaWO_4 nanophosphors are shown in Fig. 1(a) and (b), respectively. It can be confirmed that all the as-prepared and annealed samples are single phased and their diffraction peaks match well with JCPDS (Joint Committee for Powder diffractions) card no. 41-1431, $a = 5.242 \text{ \AA}$, $c = 11.373 \text{ \AA}$, $V = 312.63 \text{ \AA}^3$ and having scheelite type tetragonal structure ($I4_1/a$).

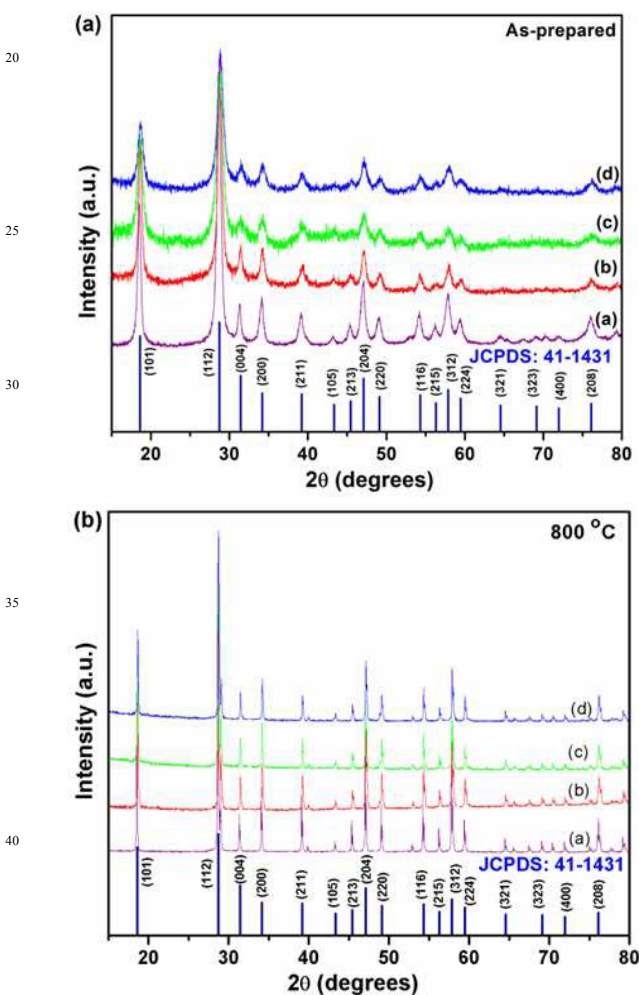


Fig. 1 XRD patterns (JCPDS No. 41-1431) of (a) as-prepared and (b) annealed at 800 °C $\text{CaWO}_4:\text{xSm}^{3+}$ nanophosphors with different concentrations of Sm^{3+} (a) $x = 2$ at.% (b) $x = 5$ at.% (c) $x = 7$ at.% and (d) $x = 10$ at.%.

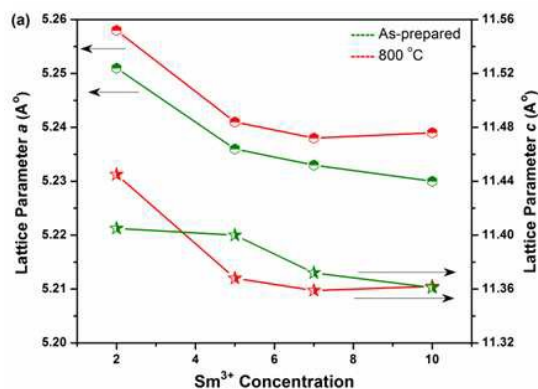
Doping concentration does not affect the diffraction patterns and crystal structure, upto 10 at.% of Sm^{3+} ion doped into CaWO_4 host matrices. This demonstrates the successful substitution of Sm^{3+} ions in the Ca^{2+} sites. Furthermore, the annealed samples have sharper peaks as compared to as-prepared samples. This shows improved crystallinity and increase in crystallite size on annealing. However, with the increase in Sm^{3+} ion concentration the intensities of diffraction peaks decrease slightly, which indicates the defects associated with the sample surface and lattice distortion which has been also confirmed in PL study (discussed later). Increase in peak intensities are also observed on annealing. As compared to pure CaWO_4 , the diffraction peaks shift towards higher 2θ with Sm^{3+} doping in CaWO_4 matrices (Fig. 1(a) and (b)). This is due to decrease in unit cell volume due to ionic radii mismatches between Sm^{3+} (0.958 Å) and Ca^{2+} (1.12 Å).²⁹

The average crystallite size D was calculated using the Scherrer equation,

$$D = \frac{0.89 \lambda}{\beta \cos \theta} \quad (1)$$

Where, D is the average crystallite size, λ is the wavelength of the X-rays (0.15405 nm), and θ and β are the diffraction angle and full-width at half maximum (FWHM) of the peaks in the XRD patterns, respectively. The strongest three peaks ($1\ 0\ 1$) at $2\theta = 18.60^\circ$, ($1\ 1\ 2$) at $2\theta = 28.72^\circ$ and ($2\ 0\ 4$) at $2\theta = 47.10^\circ$ were used to calculate the average crystallite size (D) of the prepared samples. Table 1 summarizes the average crystallite size (D), lattice parameters and cell volume of the ASP and 800 °C annealed samples of CaWO_4 with different concentrations of Sm^{3+} ions.

Fig. 2(a) and (b) show the Sm^{3+} ion concentration dependence of lattice parameters a (Å), c (Å) and unit cell volume, respectively.



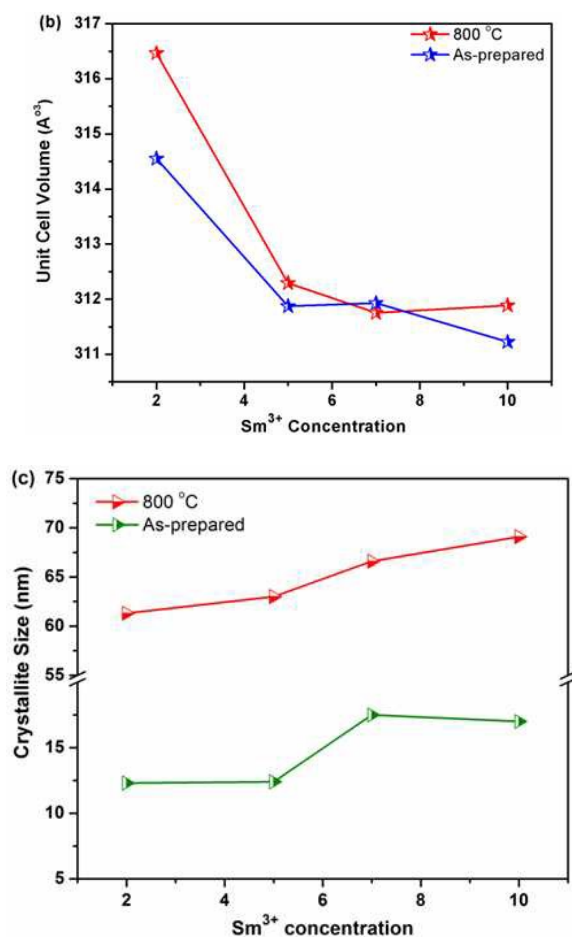


Fig. 2 (a) Lattice parameters, (b) Unit cell volume and (c) Crystallite size as a function of Sm³⁺ ions concentration.

In general, solid solutions show linear trends of lattice parameters in accordance with the ionic radius of substituted ion and its concentration.³⁰ It can be seen that with increase in Sm³⁺ ion concentration from 2 to 10 at.%, cell volume and lattice parameters decrease. Crystallite size increases with increase in Sm³⁺ concentration due to the increase in strain by the replacement of Ca²⁺ ions by Sm³⁺ ions of smaller radii (Fig. 2(c)). It is well known that the uniformity of the size and shape is controlled by nucleation³¹. In the present preparation method, reaction was started after adding ethylene glycol. During the heating process, nucleation and crystal growth continued. This may be the reason for irregular shapes and agglomerated particles. Also due to diffusion the particles get agglomerated on annealing this result in increase in crystallite size after annealing. Rothova et. al³² elaborate the relation between temperature and grain growth in their paper. Literature³³ also supports the results obtained in our work. In case of as-prepared samples crystallite size increases upto 7 at.% and then it decreases. Our results are

supported by the observations of Parchur et. al³⁴, Dutta et. al³⁵ and Singh et. al³⁶. They have also reported similar disorder in case of crystallite sizes with different doping concentration.

W-H (Williamson-Hall) fitting method was used to calculate the strain induced in nanoparticles.³⁷ The strain ϵ was estimated from the slope of the linear fit of the plot between $\beta \cos \theta / \lambda$ along the y-axis and $\sin \theta / \lambda$ along the x-axis. Linear fit to the data for ASP 10 at. % Sm³⁺ -doped CaWO₄ is shown in Fig.3.

The value of strain was found in the range ~0.0025 to 0.0045 for ASP and annealed samples. Positive slope values show the presence of tensile strain in the system. Similar behaviour has been reported for Gd³⁺ co-doped samples in CaMoO₄:Eu system.³⁸

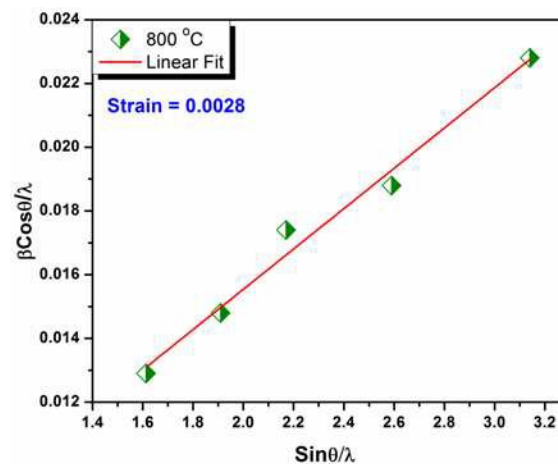


Fig. 3 Plot of $\beta \cos \theta / \lambda$ vs $\sin \theta / \lambda$ of 800 °C annealed 10 at.% Sm³⁺-doped CaWO₄ sample.

3.2 TEM Study

Morphology of the synthesized nanophosphors was examined using Transmission electron microscopy (TEM). It was observed that particles were almost spherical with average particle diameters ranging between 18-25 nm for 5 at.% Sm³⁺ -doped CaWO₄ as-prepared sample (Fig. 4(a)), which is in agreement with the calculated sizes from XRD studies (Fig. 1(a)). Fig. 4(b) shows its corresponding SAED pattern shape like fully concentric rings, implying that the products were polycrystalline. The inter planar spaces were calculated from the diameters of the rings, and compared with those of the JCPDS card no. 41-1431, which confirmed its tetragonal crystal structure. All SAED patterns show the same (004), (200), (204), (303) and (325) planes, which are in good accordance with the XRD results.

Table 1Unit cell constants, calculated average crystallite size and the strain of as-prepared and annealed at 800 °C $\text{CaWO}_4:\text{Sm}^{3+}$ nanoparticles.

Samples	Eu ³⁺ (at.%)	Cell Parameters		c/a	Cell volume (Å ³)	Crystal size (nm)
		a = b(Å)	c(Å)			
JCPDS 41-1431		5.242	11.373	2.169	312.63	
As-prepared	2	5.251	11.405	2.171	314.54	12.3
	5	5.236	11.400	2.177	311.87	12.4
	7	5.233	11.372	2.173	311.92	17.5
	10	5.230	11.361	2.172	311.22	17.0
Annealed	2	5.258	11.445	2.176	316.46	61.3
	5	5.241	11.368	2.169	312.29	63.0
	7	5.238	11.359	2.168	311.75	66.6
	10	5.239	11.362	2.168	311.88	69.1

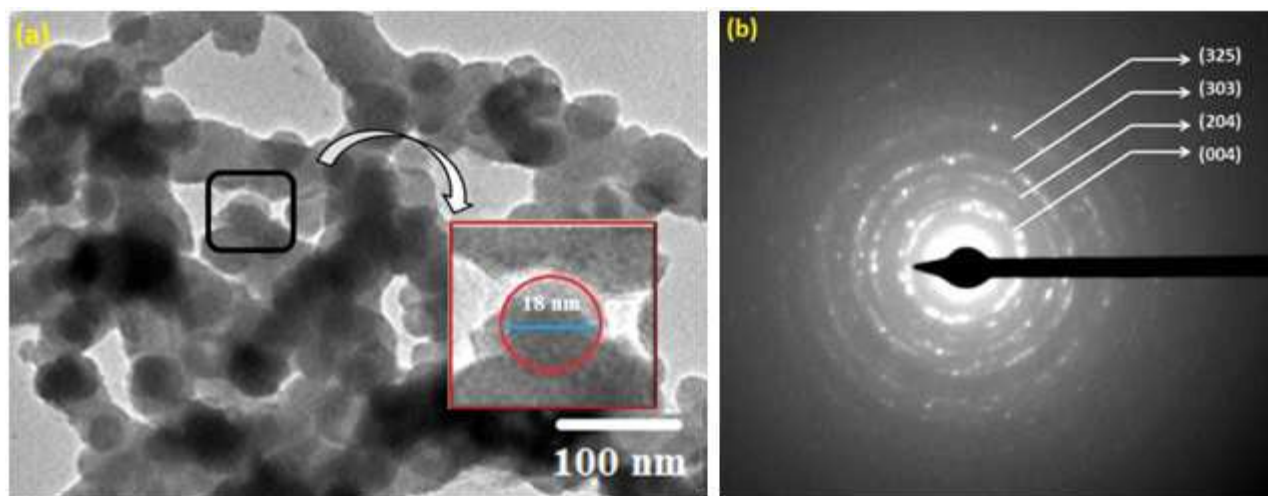


Fig. 4 (a) TEM image of as-prepared 5 at.% Sm^{3+} -doped CaWO_4 (inset shows the expanded view of a single nanoparticle having an average diameter of 18 nm) and (b) corresponding SAED pattern.

3.3 DSC/TGA Study

Fig. 5 shows the simultaneous (Differential Scanning Calorimetry/Thermal Gravimetric Analysis) DSC/TGA curves along with DTG curves of ASP 7 at.% Sm^{3+} doped CaWO_4 . The sample was measured in the temperature range of 35 to 1000 °C with a heating rate of 10 °C/min under nitrogen atmosphere. The TG analysis in **Fig. 5** presents a weight loss of 5.15% between 80 to 300 °C, 1.44% in the range 300-600 °C and no appreciable loss is observed beyond 600 °C for 7 at.% Sm^{3+} -doped CaWO_4 . The mass loss till 300 °C is attributed to complete dehydration of the powders while the mass loss till 600 °C is due to the evaporation of organic constituents like EG and methanol.

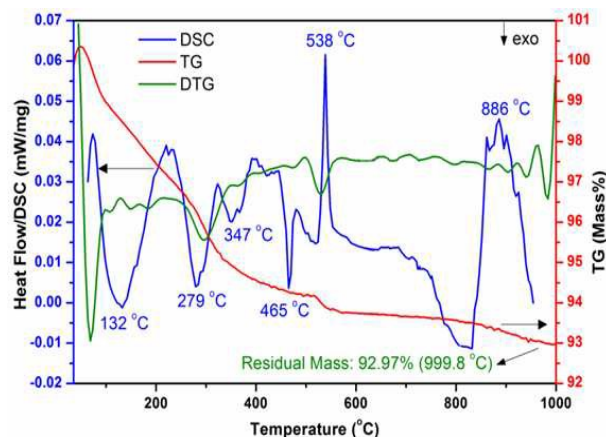


Fig. 5 Simultaneous DSC/TG character of as-prepared 7 at.% Sm^{3+} -doped CaWO_4 along with DTG.

There are three exothermic peaks in the DTA curve in the vicinity of 100 °C, 300 °C and 600 °C which correspond to evaporation of water molecules, decomposition of organic molecules and phase formation of $\text{CaWO}_4 \cdot 7\text{Sm}^{3+}$, respectively. To study the heat flow as a function of temperature in the inert gas (N_2) atmosphere associated with transitions in $\text{CaWO}_4 \cdot 7\text{Sm}^{3+}$ ASP sample DSC was recorded (Fig.5). The curve shows both exothermic and endothermic peaks. The peak around 132 °C represents the mass loss due to evaporation of water and methanol. However, the exothermic peak centred at about 279, 347 and 465 °C signifies the evaporation of organic compounds in the sample. Whereas, the large and sharp endothermic DSC (Differential Scanning Calorimetry) peaks at about 538 and 886 °C indicate the phase formation of $\text{CaWO}_4 \cdot 7\text{Sm}^{3+}$. These results show that the prepared nanophosphors are thermally stable and can be used in lighting and display devices.

3.4 Micro-Raman spectroscopy study

Fig. 6 shows Raman spectra at 633 nm in the frequency ranging from 100 to 1100 cm^{-1} for $\text{CaWO}_4 \cdot \text{Sm}^{3+}$ ($\text{Sm}^{3+} = 2, 5, 7$ and 10 at.%) nanoparticles synthesized by the Polyol method and annealed at 800 °C.

The Raman bands observed at $\sim 114, 210, 332, 398, 796, 836$ and 912 cm^{-1} are related to CaWO_4 tetragonal phase. Among them, there are 3 A_g vibrations (210, 332 and 912 cm^{-1}), five B_g (86, 218, 332, 401 and 836 cm^{-1}) and five E_g (114, 190, 274, 409 and 796 cm^{-1}).^{39(a)} The peak located at 912 cm^{-1} can be attributed to symmetric stretching (ν_1) of W-O while the peak at 332 cm^{-1} is assigned to the symmetric bending (ν_2) of O-W-O. The peaks at 796 and 836 cm^{-1} are attributed to O-W-O anti-symmetric stretching (ν_3) while peaks at 398 and 409 cm^{-1} are assigned to W-O anti-symmetric bending (ν_4).^{39(a)-(c)} The peaks at 190 and 274 cm^{-1} are related to free rotation modes (ν_{fr}) of WO_4 group. According to literature data,^{40,41} all Raman modes observed for $\text{CaWO}_4 \cdot \text{Sm}^{3+}$ obtained in this work are characteristics of the tetragonal structure.

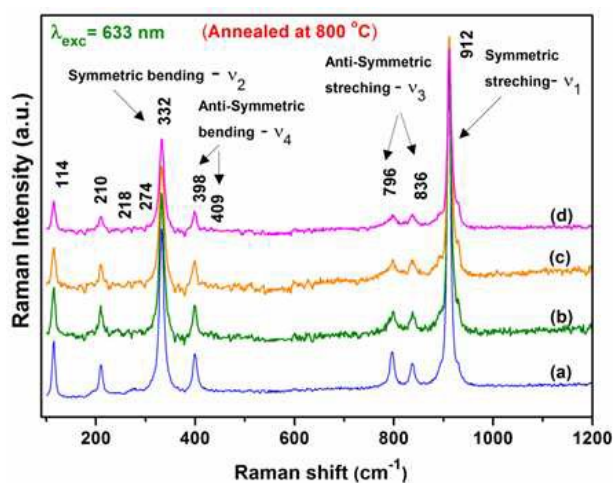


Fig. 6 Room temperature Raman spectra of $\text{CaWO}_4 \cdot x\text{Sm}^{3+}$ nanopowders (a) $x=2$ at.% (b) $x=5$ at.% (c) $x=7$ at.% and (d) $x=10$ at.% processed by the polyol method and treated at 800 °C for 2 h

The stretching, torsion and bending vibrational modes of

W-O bonds were not affected by the doping concentration of Sm^{3+} ion, since the Sm^{3+} ion replaces the Ca^{2+} ion which is located at A site while W atom is located at B site in the scheelite structure of CaWO_4 matrix.⁴²

3.5 FTIR study

Fig. 7 Shows the FT-IR spectra of ASP and 800 °C annealed 7 at.% Sm^{3+} -doped CaWO_4 in the wavenumber range of 400-4000 cm^{-1} . The scheelite type structures have 26 modes of vibrations (Raman + Infrared) which can be shown as:

$$\Gamma(\text{Raman} + \text{Infrared}) = 3A_g + 5A_u + 5B_g + 3B_u + 5E_g + 5E_u \quad (2)$$

Where, A_g , B_g and E_g are 13 Raman active modes while the odd modes $4A_u$ and $4E_u$ are 8 Infrared active modes. The three B_u vibrations are silent modes whereas one A_u and one E_u modes are acoustic vibrations.⁴³

There are two peaks at 1670 and 3510 cm^{-1} implying H-O-H bending and O-H stretching vibrations, respectively. This is due to the presence of water molecules on the surface of the nanoparticles. These peaks are absent in case of annealed samples due to the evaporation of adsorbed water. The strong absorption peak at 850 cm^{-1} can be assigned to anti symmetric stretching vibration (ν_3) due to O-W-O bond in WO_4^{2-} tetrahedron. The peak at 445 cm^{-1} can be assigned to bending vibration (ν_2) of O-W-O bond. The peaks at 850 and 445 cm^{-1} shifted slightly towards lower wave number by $\sim 10-15 \text{ cm}^{-1}$ due to the expansion in lattice of CaWO_4 host on annealing at 800 °C. Similar behaviour was also observed in literature.⁴⁴ The presence of C-H stretching vibration from EG molecules adsorbed on the surface of nanoparticles can be observed by the peak at 2928 cm^{-1} in the as-prepared samples. Thus, the single phase scheelite structure of $\text{CaWO}_4 \cdot \text{Sm}^{3+}$ phosphors are also confirmed by FT-IR studies.

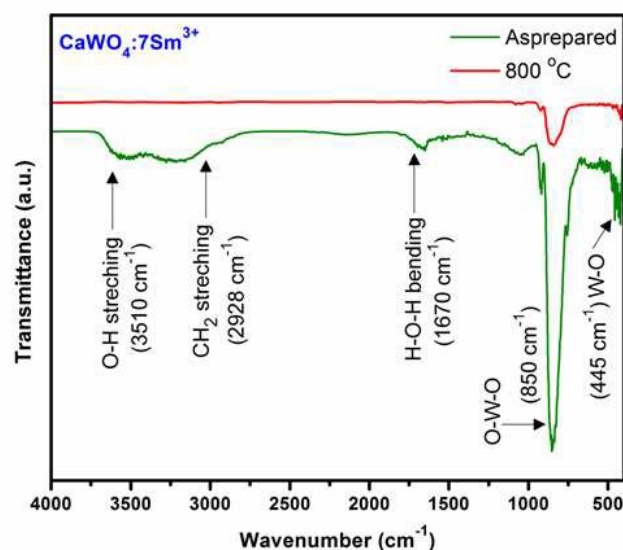


Fig. 7 FTIR spectra of as-prepared and 800 °C annealed 7 at.% Sm^{3+} -doped CaWO_4 nanophosphor.

3.6 XPS Study

In order to investigate the chemical composition and valence states of the material, a well known X-ray photon spectroscopy

(XPS) technique has been employed. Observed data of all elements were charge corrected with respect to C1s, which appears at 284.6 eV. C1s appears mainly due to adventitious carbon during the atmospheric exposure. The survey scan of core binding energy (BE) of Ca, W, O and Sm in the range 0-1100 eV has been shown in the Fig. 8(a). Fig. 8(b) shows the XPS spectra of Ca(2p) obtained in the range 343- 355 eV. The peak corresponding to Ca (2p) had a core binding energy of ~346.78 eV ($2p_{3/2}$) and 350.41 eV ($2p_{1/2}$) having FWHM of 1.9 and 2.2 eV, respectively. These results confirm the formal oxidation state +2 of Ca.³⁸ XPS spectra of W (4f) has been observed in the range 20-36 eV (Fig. 8(c)). The peak corresponding to W(4f) had a core BE of 30.97 eV ($4f_{7/2}$) and 33.18 eV ($4f_{5/2}$) with FWHM of 2.5 and 2.28 eV, respectively.⁴⁵

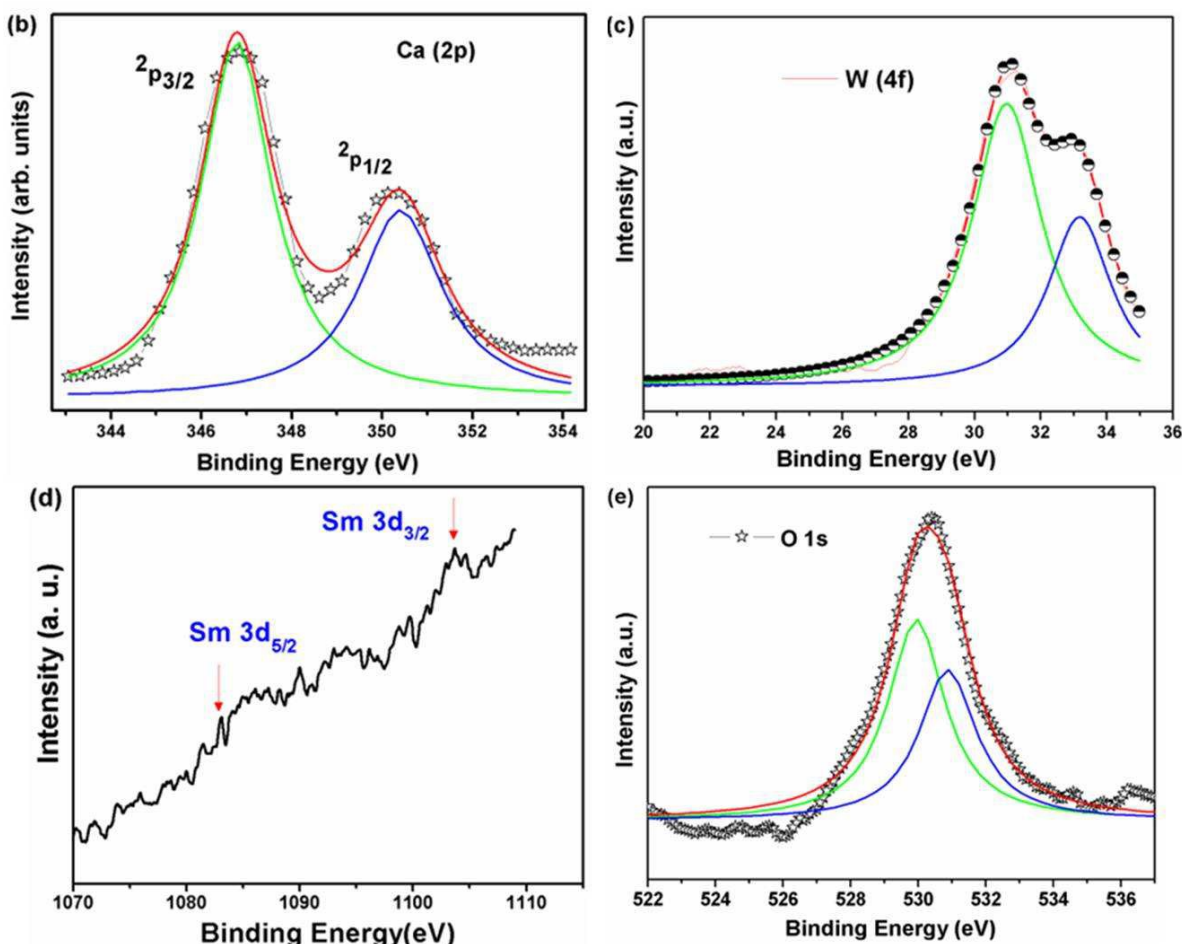
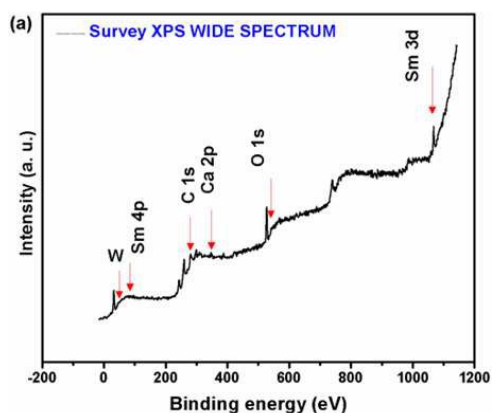


Fig. 8 (a) XPS survey spectra of CaWO_4 . Peaks corresponding to the core binding energies of individual elements viz, Ca, W and Sm are shown in Fig. (b), (c) and (d), respectively, (e) XPS spectra of O1s for 800 °C annealed CaWO_4 :5 at.% Sm^{3+} .

XPS spectra of Sm (3d) have been shown in Fig. 8(d). Peak corresponding to 1082.34 and 1107.56 eV corresponds to $3d_{5/2}$ and $3d_{3/2}$, respectively. The XPS study clearly reveals the presence of different elements involved in the Sm doped CaWO_4 nanoparticles.⁴⁶ The XPS spectrum of O1s is used as a probe for investigating the presence of oxygen ion vacancies on the surface of the sample and has been shown in Fig. 8(e). The peaks were de-convoluted using Lorentzian function. The two peaks well fitted to B.E.~529.9 and 530.8 eV with FWHM ~2.03 and 2.04

eV, respectively.

3.7 UV Study

The energy band gap for ASP and 800 °C annealed 5 at.% Sm^{3+} -doped CaWO_4 nanoparticles was calculated by the plot between $(\alpha h\nu)^2$ and $h\nu$ (Fig. 9) using the relation given by Wood and Tauc.⁴⁷

$$\alpha h\nu = k(h\nu - E_g)^n \quad (3)$$

Where, k is a constant, α is the absorbance, h is the Planck's constant, ν is the frequency, E_g is the optical band gap and exponent n has the value $1/2$ since the tungstates have an optical absorption governed by direct electronic transitions due to its straight line behavior in the high energy region.⁴⁸ Therefore, the energy gap was calculated by extrapolation of the linear portion of the $(\alpha h\nu)^2$ versus $h\nu$ curve to zero absorption coefficient value.

It was found that the energy gaps for ASP and 800 °C annealed 5 at.% Sm³⁺ doped CaWO₄ are 4.64 and 4.38 eV, respectively. Fig. 9 shows that energy gap decreases on annealing, which can be associated with the intermediate localized states in the band gap due to structural defects.⁴⁹ The band gap calculations for 800 °C annealed CaWO₄:Sm³⁺ (Sm³⁺ = 2, 7 and 10 at.%) nanoparticles are shown in electronic supplementary information (ESI†) Fig.S1(a)-(c) and estimated to be ~ 4.48, 4.46 and 4.19 eV.

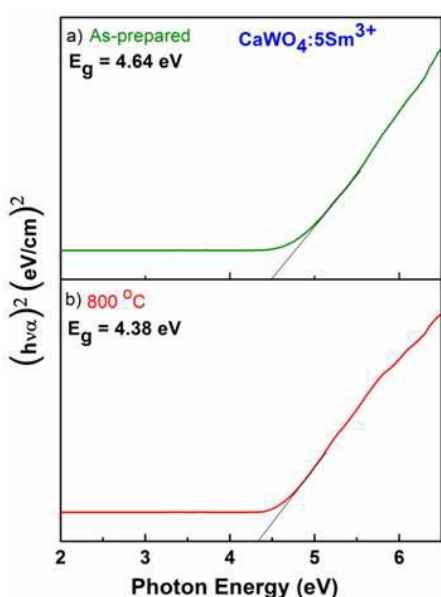


Fig. 9 Variation of $(\alpha h\nu)^2$ vs photon energy (in eV) curve for (a) as-prepared and (b) 800 °C annealed 5 at.% Sm³⁺-doped CaWO₄.

55

3.8 Photoluminescence study

3.8.1 Excitation Study

Fig. 10 (a) and (b) show the excitation spectra of as-prepared and 800 °C annealed samples of CaWO₄:Sm³⁺ (2, 5, 7 and 10 at.%) monitored at 605 nm. It contains an intense broad band (220-290 nm) with the maximum intensity around 255 nm, which is assigned to the overlap of charge transfer (CT) absorption from the oxygen ligands to the central tungsten atom ($O^{2-} \rightarrow W^{6+}$) within the WO_4^{2-} groups and also from oxygen ligands to the samarium ions ($O^{2-} \rightarrow Sm^{3+}$).^{17,50}

The f-f forbidden transitions of Sm³⁺ ions around ~345 nm ($^6H_{5/2} \rightarrow ^4K_{17/2}$), 363 nm ($^6H_{5/2} \rightarrow ^4H_{7/2}$), 376 nm ($^6H_{5/2} \rightarrow ^6P_{7/2}$), 403 nm ($^6H_{5/2} \rightarrow ^4F_{7/2}$), 420 nm ($^6H_{5/2} \rightarrow ^6P_{5/2}$), 439 nm ($^6H_{5/2} \rightarrow ^4G_{9/2}$), 463 nm ($^6H_{5/2} \rightarrow ^4I_{13/2}$) and 481 nm ($^6H_{5/2} \rightarrow ^4I_{11/2}$) are clearly observed in the longer wavelength region (Fig. 10 (a) and (b)). It indicates that CaWO₄ can act as efficient host and can sensitize Sm³⁺ with an energy transfer from WO_4^{2-} groups to Sm³⁺ ions in CaWO₄:Sm³⁺ phosphors. It was observed in the excitation spectra that in case of as-prepared samples the luminescence intensity decreases with increase in Sm³⁺ ion concentration (Fig. 10 (a)), it is due to concentration quenching effect while in case of annealed samples the luminescence intensity decrease till 7 at.% of Sm³⁺ (Fig. 10 (b)) and then it shows some increase due to decrease in non-radiative rates by the removal of OH molecules on annealing at 800 °C. The peak intensities corresponding to Sm³⁺ ion are relatively high in case of annealed samples than the as-prepared samples, which corroborates the decrease in non-radiative processes arising from -OH molecules on the surface of the nanoparticles.

In case of 800 °C annealed 2 at.% Sm³⁺-doped CaWO₄, the absorption intensity of Sm/W-O CT absorption is 2.6 times stronger than $^6H_{5/2} \rightarrow ^4F_{7/2}$ transition at 403 nm (FWHM~ 4.28 nm) which suggests a strong energy transfer from Sm/W-O CT band to Sm³⁺ ions (Fig.10 (c)).

Cite this: DOI: 10.1039/c0xx00000x

www.rsc.org/njc

PAPER

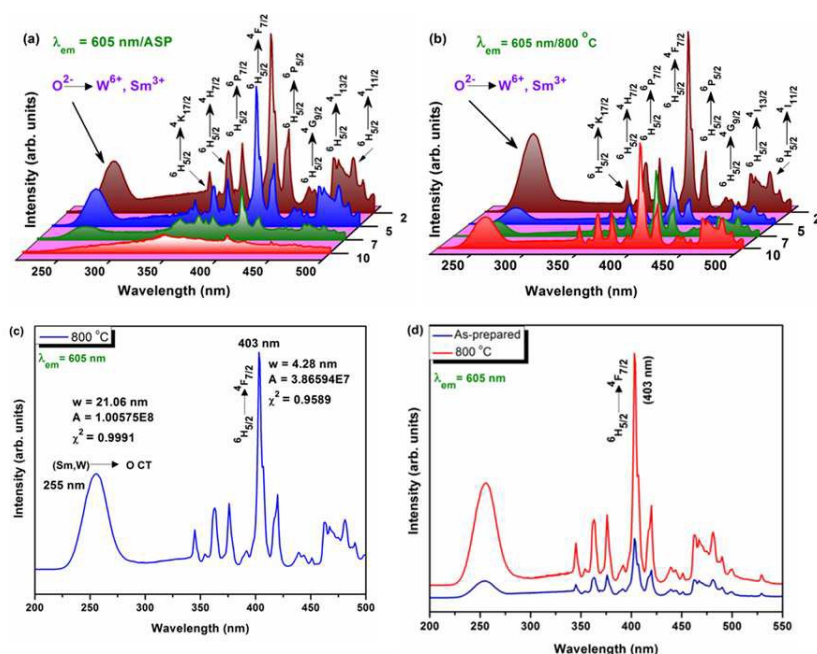


Fig. 10 Excitation spectra of (a) as-prepared, (b) 800 °C annealed Sm^{3+} ($\text{Sm}^{3+}=2, 5, 7$ and 10 at.%) doped CaWO_4 nanoparticles under 605 nm excitation, (c) Excitation spectra of 2 at.% Sm^{3+} -doped CaWO_4 nanophosphor annealed at 800 °C and (d) Excitation spectra (after excitation at 605 nm) of 7 at.% Sm^{3+} doped CaWO_4 nanoparticles for as-prepared and 800 °C annealed samples.

5

Fig. 10 (d) shows the excitation spectra of ASP and 800 °C annealed 7 at.% Sm^{3+} -doped CaWO_4 nanophosphors at 605 nm emission wavelength. The position of Sm/W-O charge-transfer band (CTB) is shifted to higher wavelength by ~2-5 nm due to annealing of the samples at 800 °C than in ASP samples; similar observations have been reported in Mo-O CTB.⁵¹

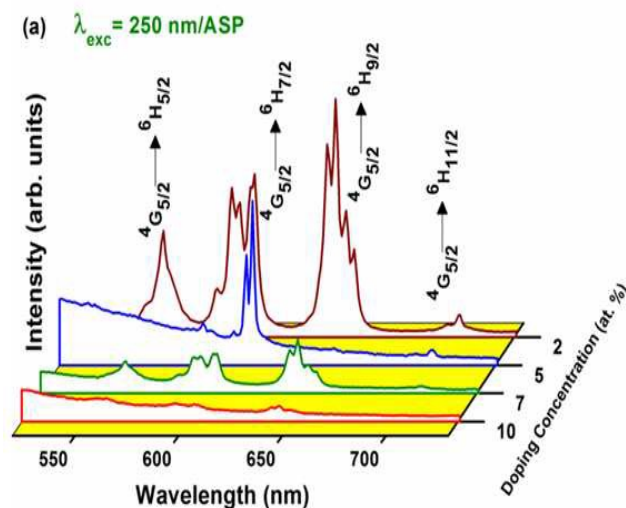
This can be explained as follows: when an electron is transferred from oxygen to W, an electronic transition takes place which gives rise to the W-O charge transfer band (CTB). In ASP samples, there are a relatively large number of dangling bonds over the particle surface and the lattice is less ordered as compared to that of annealed samples. There is also a higher degree of ionic bonding between W and O for the as-prepared samples as compared to that for 800 °C annealed samples, and this result in lower energy absorption for annealed samples. Consequently, the position of the W-O charge-transfer band is shifted to higher wavelength by ~2-5 nm upon annealing of the samples at 800 °C compared with the as-prepared samples.

The luminescence intensity for $6\text{H}_{5/2} \rightarrow 4\text{F}_{7/2}$ transition at 403 nm of 800 °C annealed sample increases by 6 times as compared to ASP sample of $\text{CaWO}_4:7\text{Sm}^{3+}$. This may be due to decrease in H_2O molecules, non-radiative rates arising from OH group and EG molecules on the surface of the nanoparticles. **Fig. S2†(a),(b)**, (see ESI†) shows the excitation spectra of as-prepared and 800 °C annealed samples of CaWO_4 with different Sm^{3+} (2, 5, 7 and 10

30 at.%) ions concentration monitored at 644 nm and it is also showing the same pattern as shown by the excitation spectra monitored at 605 nm (**Fig. 10**).

35 **3.8.2 Emission study**

Fig. 11 (a) and **(b)** show the emission spectra of Sm^{3+} (2, 5, 7 and 10 at.%) -doped CaWO_4 as-prepared samples under excitation at 250 nm (host or W-O CTB).



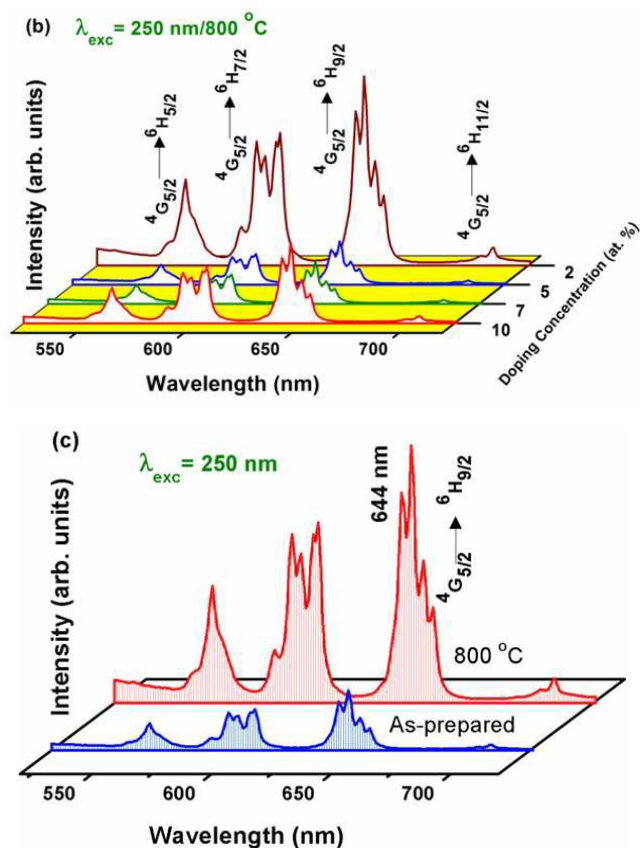


Fig. 11 Emission spectra of (a) as-prepared and (b) 800 °C annealed Sm^{3+} ($\text{Sm}^{3+} = 2, 5, 7$ and 10 at.%) doped CaWO_4 nanoparticles under 250 nm excitation and (c) Emission spectra (after excitation at 250 nm) of 2 at.% Sm^{3+} doped CaWO_4 nanoparticles for as-prepared and 800 °C annealed samples.

Fig. 12 (a) and (b) show the emission spectra under 405 nm (direct Sm^{3+}) excitation. The PL spectra show four strong emission peaks at $561, 605, 644$ and 703 nm, which originates from ${}^4\text{G}_{5/2} \rightarrow {}^6\text{H}_{5/2}, {}^4\text{G}_{5/2} \rightarrow {}^6\text{H}_{7/2}, {}^4\text{G}_{5/2} \rightarrow {}^6\text{H}_{9/2}$ and ${}^4\text{G}_{5/2} \rightarrow {}^6\text{H}_{11/2}$ transitions of Sm^{3+} , respectively. It can be observed from the PL spectra that the doping concentration of Sm^{3+} has no effect on the spectra profile except for luminescence intensity. In the emission spectra the strongest peaks are visible at 644 nm and the samples show a predominant orange red emission of the characteristic Sm^{3+} (${}^4\text{G}_{5/2} \rightarrow {}^6\text{H}_{9/2}$) transition. The emission spectra of $\text{CaWO}_4:\text{Sm}^{3+}$ ($2, 5, 7$ and 10 at.%) under 364 and 377 nm excitation show similar behaviour (Fig. S3, see ESI †).

The emission lines around 561 nm originates due to magnetic dipole transition (${}^4\text{G}_{5/2} \rightarrow {}^6\text{H}_{5/2}$) while the ${}^4\text{G}_{5/2} \rightarrow {}^6\text{H}_{9/2}$ lines around 644 nm originate due to electric dipole transition (Fig. 11 (a) and (b)). The luminescence intensity of electric dipole transition is greater than the magnetic dipole transition which shows that Sm^{3+} ions occupied the sites without inversion symmetry in the host lattice.

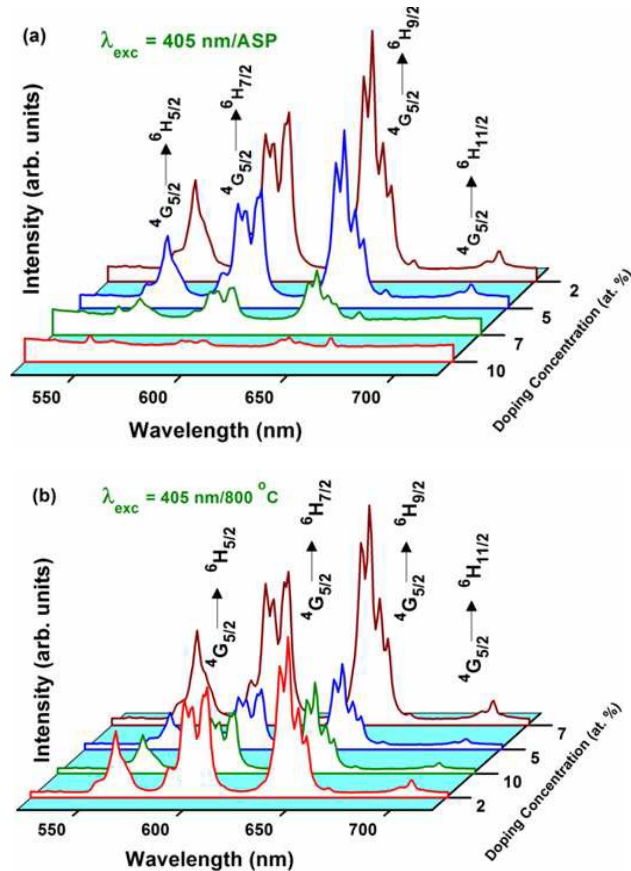


Fig. 12 Emission spectra of (a) as-prepared and (b) 800 °C annealed Sm^{3+} ($\text{Sm}^{3+} = 2, 5, 7$ and 10 at.%) doped CaWO_4 nanoparticles under 405 nm excitation.

The effect of annealing on the luminescence properties of synthesized phosphors was also studied and it was found that annealing enhances the luminescence intensity due to decrease in non-radiative rates, removal of $-\text{OH}$ molecules from the surface of nanoparticles and also due to decrease of lattice defects which results in the increase in energy transfer from WO_4^{2-} to Sm^{3+} and hence emission intensity increase.

Excitation wavelength^{4(g)} and annealing temperature^{4(g)} are the parameters which influence the luminescence intensity. It was observed that in case of as-prepared samples the optimum concentration was 2 at.% while in case of 800 °C annealed samples it was 7 at.% (Fig. 12(a) and 12(b)). This is due to the decrease of mean distance between the neighbouring lanthanide ions below the critical value, which leads to cross-relaxation among them and thus probability of radiative transition is reduced.⁵² After annealing the occupancy of Sm^{3+} ions in the Ca^{2+} lattice sites increases, which results in the reduction of non-radiative rates and improvement of crystallinity. This increases the optimum concentration. Our results are supported by the observations reported in literature.^{51,53(a),(b)} They have reported similar disorder in case of samples annealed at higher temperatures.

Fig. 11 (c) shows the emission spectra of ASP and 800 °C annealed samples of 2 at.% Sm^{3+} doped CaWO_4 nanophosphors. The excitation wavelength used was 250 nm. It was observed that the relative intensity of Sm^{3+} with respect to the ASP sample under 644 nm peak increases up to ~ 5 times on annealing the

sample at 800 °C. The doping concentrations of dopants play an important role on the luminescent properties of phosphors. It can be clearly found that the Sm³⁺ doping concentration has no effect on the spectra profile except for intensity. This is due to the shielding of 4f electrons of trivalent rare earth elements by the outer 5s and 5p electrons.¹³ Thus, the f–f transitions of trivalent lanthanides are weakly affected by the crystal field.

In order to obtain the optimal concentration of Sm³⁺ ion in the CaWO₄ host lattice, we have prepared samples with different Sm³⁺ ion concentration. From the emission spectra (Fig. 11(a) and 12(a)), it can be observed that 2 at.% Sm³⁺-doped CaWO₄ showed the highest luminescence then the luminescent intensity decreases sharply with further increase in Sm³⁺ ion concentration.

This decrease in the emission intensity shows the occurrence of energy migration between Sm³⁺ in different sites in the lattice by non-radiative transitions, resulting in concentration quenching. Exchange interaction, radiation reabsorption, or multipole–multipole interaction are the processes by which non-radiative energy transfer from one Sm³⁺ ion to another Sm³⁺ ion occur.⁵⁴ Blase⁵⁵, suggested that if the activator is introduced solely on Z-ion sites, N is the number of Z ions in the unit cell and V is the volume of the unit cell, x_c is the critical concentration, then there is on the average one activator ion per V/x_cN. The critical transfer distance (R_c) that is the critical separation between the donor (activator) and acceptor (quenching site) is approximately equal to twice the radius of a sphere with the volume, and it can be calculated by the critical concentration of the activator ion as follows:⁵⁶

$$R_c = 2 \left[\frac{3V}{4\pi x_c N} \right]^{1/3} \quad (4)$$

In our case, by taking x_c = 0.02, N = 4 and V = 312.63 Å³, the critical distance R_c are found to be ~ 19.58 and 19.62 Å for ASP and 800 °C annealed 2 at.% Sm³⁺-doped CaWO₄, respectively. Therefore, the energy transfer in the present case will occur only by electric multipolar interaction.⁵⁷

Van Uitert has studied the energy transfer interactions between rare earth ions. In Van Uitert's model the relationship between the luminescent intensity (I) and the doping concentration (C) can be expressed as below:^{58,59}

$$I(C) = \frac{C}{K(1 + \beta C^{Q/3})} \quad (5)$$

Where, C is concentration of donor, K and β are constants for a certain system, Q represents the interaction type between donors, here Q= 3, 6, 8 or 10, indicating the exchange interaction, electric dipole–dipole, electric dipole–quadrupole, or electric quadrupole–quadrupole interactions, respectively. A nonlinear fitting by using the formula $y = ax/(1 + bx^c)$ was carried out on the concentration quenching data shown in Fig. 13 with the same form as Eq.(5). The value of c after nonlinear fitting comes to be 1.95, which means that Q is approximately 6. Thus, the main mechanism for the luminescence quenching of Sm³⁺ ions in CaWO₄ nanophosphors is the electric dipole–dipole interaction

between Sm³⁺ ions.

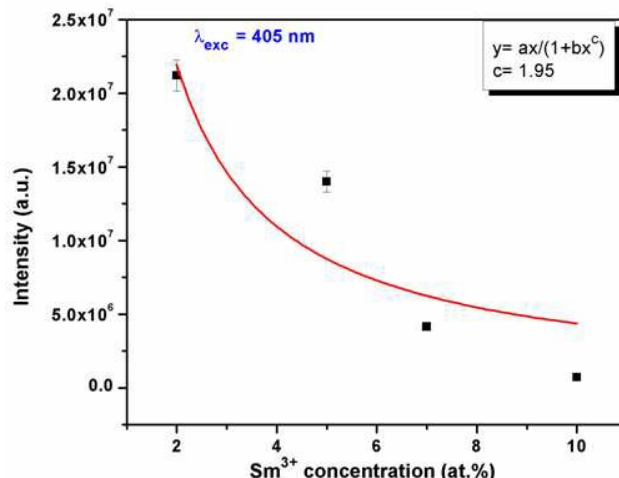


Fig. 13 Dependence of integrated emission intensity of ⁴G_{5/2} → ⁶H_{9/2} transition (644 nm) on the doping concentration of Sm³⁺ in CaWO₄:Sm³⁺ phosphors. The blue circle points show the experimental data, red solid line represents the fitting curve to the formula $y = ax/(1+bx^c)$ by using Van Uitert's model.

The surface defects of the nanoparticles or the WO₄²⁻-groups may be the quenching centers. Generally speaking, the energy transfer between rare earth ions is an energy migration process: the Sm³⁺ ions at excited state ⁴G_{5/2} transfer their energies to the Sm³⁺ ions at ground state, and then the formers back to ground state and the latter get into ⁴G_{5/2} state. For an energy migration process, Q should be equal to 3. Therefore, the Sm³⁺ ions cannot serve as the quenching centers of their own in CaWO₄ nanophosphors.

3.9 CIE and CCT values

Fig. 14 (a) and (b) show the Commission Internationale de l'Eclairage (CIE) chromaticity diagram for CaWO₄:Sm³⁺(Sm³⁺ = 2, 5, 7 and 10 at.%) ASP and annealed at 800 °C phosphors excited at 250 and 405 nm, respectively. The calculated CIE color coordinates for all samples are listed in Table 2. Under 405 nm excitation, a red-orange light was observed for all samples. By changing the excitation wavelength^{4(g),60} and also the Sm³⁺ ion concentration, the CIE chromaticity coordinates vary from (0.26, 0.37, presented by point a4) to (0.29, 0.28, presented by point a1) and eventually to (0.45, 0.32, presented by point b1).

It clearly indicates that the color is tunable from green to bluish white, even to orange-red in the visible spectral region (Fig. 14 (b)). The emission in blue and green region is due to host CaWO₄. The host emission is dominant in case of host or W-O CTB excitation at 250 nm, while for direct excitation at 405 nm the emission is from Sm³⁺ ions.

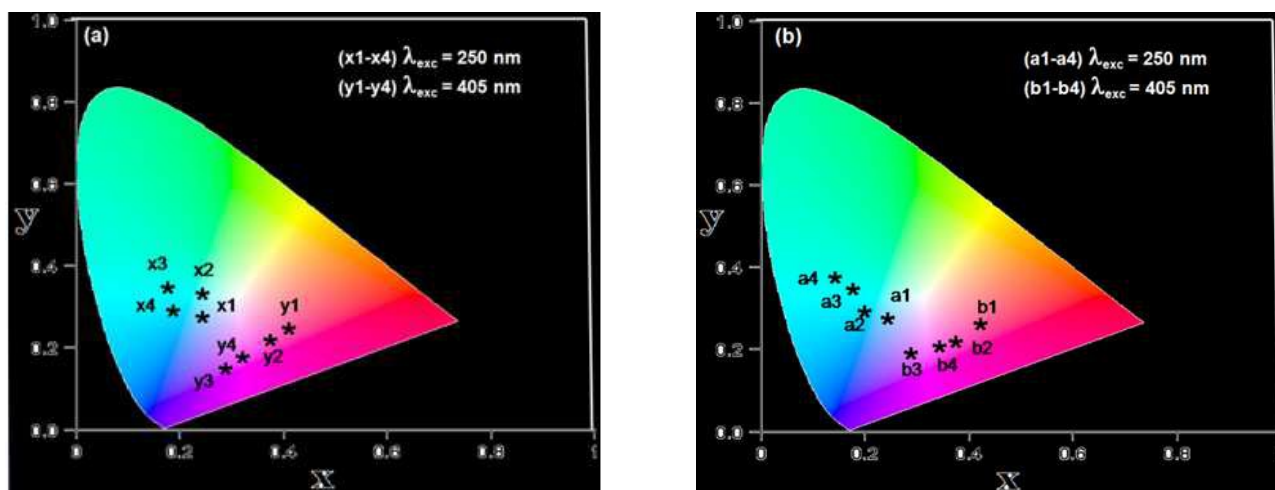


Fig. 14 The Commission Internationale de l'Eclairage (CIE) chromaticity coordinates for (a) as-prepared and (b) 800 °C annealed samples under 5 different (250 and 405 nm) excitations.

Table 2

CIE values for different concentrations of Sm^{3+} doped CaWO_4 phosphors under 250 and 405 nm excitation.

Excitation (nm)	Sm^{3+} (at.%)	CIE coordinates					
		As-prepared			Annealed (800 °C)		
		No.	X	Y	No.	X	Y
250 nm	2	x1	0.21	0.40	a1	0.29	0.28
	5	x2	0.24	0.37	a2	0.19	0.41
	7	x3	0.12	0.44	a3	0.21	0.38
	10	x4	0.11	0.39	a4	0.26	0.37
405 nm	2	y1	0.39	0.28	b1	0.43	0.30
	5	y2	0.37	0.26	b2	0.37	0.26
	7	y3	0.28	0.25	b3	0.45	0.32
	10	y4	0.24	0.19	b4	0.39	0.27

The quality of white light is calculated using McCamy empirical formula in terms of Color Correlated Temperature (CCT) values, which is expressed as:⁶¹

$$\text{CCT} = -449n^3 + 3525n^2 - 6823n + 5520.33 \quad (6)$$

Where, $n = (x - x_e)/(y - y_e)$ is the inverse slope line, $x_e = 0.332$ and $y_e = 0.186$.

The CCT values for as-prepared and 800 °C annealed samples are found to be in the range of ~1950-2900 K for different Sm^{3+} ion concentrations under 405 nm excitation. CCT values for 800 °C annealed samples are greater than the as-prepared samples due to host emission contribution. The typical CCT value for 800 °C annealed 5 at.% Sm^{3+} doped sample under 405 nm excitation is found to be 2885 K (warm white light). It suggests that color temperature of $\text{CaWO}_4:\text{Sm}^{3+}$ nanophosphors can be controlled by changing the dopant concentration and by annealing the samples.

3.10 Lifetime study

The lifetime decay curves of 2 at.% Sm^{3+} -doped CaWO_4 samples recorded under 355 nm excitation by monitoring the emission of orange red band at 644 nm, are shown in Fig.15. The reduction of population of higher energy states to 1/e of its initial population which is associated to the transitions from higher energy to the lower energy states is termed as the lifetime decay.⁶²

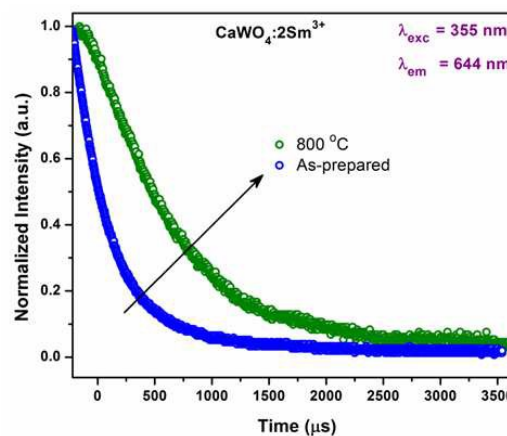


Fig. 15 Luminescence decay spectra of as-prepared and 800 °C annealed 2 at.% Sm^{3+} -doped CaWO_4 nanoparticles under 355 nm excitation.

The decay curves were fitted with both monoexponential and biexponential equations. The monoexponential decay fit is expressed as:

$$I = I_0 e^{-t/\tau} \quad (7)$$

Where, I_0 and I are intensities at zero time and at time t , respectively, and τ is the lifetime for the transition.

And the bi-exponential function is expressed as:

$$I = A_1 e^{-t/\tau_1} + A_2 e^{-t/\tau_2} \quad (8)$$

Where, τ_1 and τ_2 are the fast and slow components of the luminescence lifetimes, A_1 and A_2 are fitting parameters. Of the two exponential fits, the biexponential equation fits better than the monoexponential one, that is, the goodness of fits of parameters for ASP 2 at.% Sm^{3+} doped CaWO_4 with mono- and bi-exponential equations were found to be 0.99823 and 0.99945, respectively. This is due to the inhomogeneous distribution of the dopant ions in the host material and the transfer of excitation energy from donor to lanthanide activators.

The bi-exponential fitting of as-prepared and annealed at 800 °C 2 at.% Sm^{3+} doped CaWO_4 phosphor under 355 nm excitation are shown in Fig. 16 (a) and (b). Further, the average decay lifetimes can be calculated as:

$$\tau_{av} = \frac{I_1 \tau_1 + I_2 \tau_2}{I_1 + I_2} \quad (9)$$

The lifetime value of annealed sample (0.764 ms) (Fig. 16 (b)) is greater than the as-prepared sample (0.444 ms) (Fig. 16 (a)). This may be due to increase in particle size and reduction in surface defects after annealing, also reduction in non-radiative rates and removal of OH molecules from the surface of the nanoparticles after annealing.

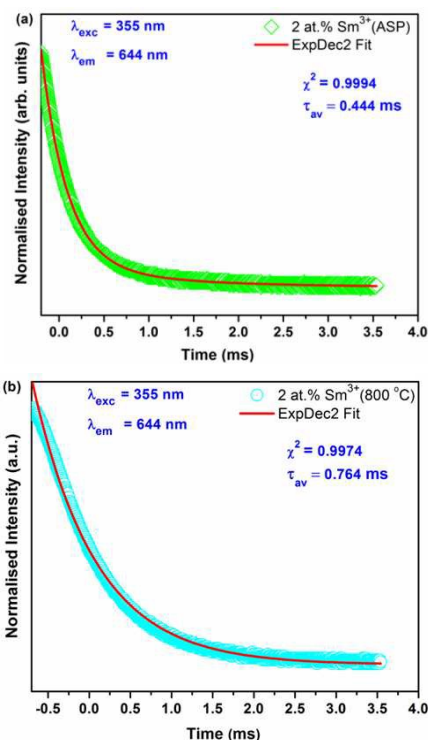


Fig. 16 Bi-exponential fitting to the decay curve ($\lambda_{em} = 644$ nm) of 2 at.% Sm^{3+} -doped CaWO_4 (a) As-prepared and (b) 800 °C annealed samples under 355 nm excitation.

Our results are supported by literature^{4(g),63,64} that after annealing the lifetime of phosphors increases. The fitted parameter (I_1 , τ_1 , I_2 , τ_2 , τ_{av} and χ^2) obtained using bi-exponential decay equation for ASP and 800 °C annealed 2 at.% Sm^{3+} -doped CaWO_4 under 355 nm are given in Table 3. The average lifetimes of 800 °C annealed Sm^{3+} ions in $\text{CaWO}_4 \cdot x$ at.% Sm^{3+} ($x = 5, 7$ and 10) were determined to be 0.515, 0.449 and 0.414 ms, respectively. It is found that the intensity of decay counts decreases with Sm^{3+} ion concentration. This may be due to concentration quenching effect.

Table 3 Parameters obtained after bi-exponential fit to the decay data of as-prepared and 800 °C annealed 2 at.% Sm^{3+} -doped CaWO_4 samples under 355 nm excitation.

Sample	Excitation (nm)	I_1 (%)	τ_1 (ms)	I_2 (%)	τ_2 (ms)	χ^2
ASP	355	42	0.28±0.0022	58	1.31±0.0016	0.9994
Annealed	355	48	0.76±0.0009	52	0.76±0.048	0.9974

4. Conclusions

Sm^{3+} ($\text{Sm}^{3+} = 2, 5, 7$ and 10 at.%) -doped CaWO_4 nanophosphors were prepared by polyol method. From photoluminescence study, it corroborates that luminescence intensity shows the optimum emission for 2 at.% doped Sm^{3+} concentration, while for higher concentration it shows decrement due to the concentration quenching. The optical band gap values for ASP and 800 °C annealed 5 at.% Sm^{3+} -doped CaWO_4 nano-particles were 4.64

and 4.38 eV, respectively. Emission spectra show the four strong emission peaks under 250, 364, 377 and 405 nm at 561, 605, 644 and 703 nm, which originates from ${}^4G_{5/2} \rightarrow {}^6H_{5/2}$, ${}^4G_{5/2} \rightarrow {}^6H_{7/2}$, ${}^4G_{5/2} \rightarrow {}^6H_{9/2}$ and ${}^4G_{5/2} \rightarrow {}^6H_{11/2}$ transitions of Sm^{3+} , respectively. The luminescence concentration quenching of Sm^{3+} doped CaWO_4 nanophosphors were studied based on the Van Uitert's model, and it was found that the electric dipole-dipole interaction is the dominant energy transfer mechanism between Sm^{3+} ions in the $\text{CaWO}_4 \cdot \text{Sm}^{3+}$ ($\text{Sm}^{3+} = 2, 5, 7$ and 10 at.%) nanophosphors.

The color coordinates for 800 °C annealed 2 at.% Sm³⁺ doped CaWO₄ phosphor were calculated to be (0.45, 0.32). The ratio of blue to yellow/orange/red intensities can bring many colours. These phosphors will be useful in production of light emitting diodes (LEDs) based on 250 nm excitation. When phosphors (CaWO₄:Sm³⁺) are coated over Hg lamp, this can produce bluish to white colors. Due to the strong blue and orange-red emission in visible region under different excitations, these nanophosphors can be potential candidates to be used in white LEDs.

10 Acknowledgements

Authors are thankful to UGC DAE Consortium for Scientific Research, Indore for TEM and XRD characterization. We are thankful to Sophisticated Instrument Laboratory of the University for providing various characterization facilities. One of the authors (Maheshwary) acknowledges the Central Research Fellowship provided by University Grants Commission (UGC), Govt. of India.

^aDepartment of Physics, Dr. Harisingh Gour University, Sagar, M. P., 470003 (India). Email: maheshwarysingh@gmail.com

^bDepartment of Physics, Indian Institute of Technology (BHU), Varanasi, 221005 (India). Email: bheeshmapratap@gmail.com

*Corresponding author: Prof. R. A. Singh, Department of Physics, Dr. Harisingh Gour University, Sagar, M. P., 470003, India, Tel: +91

9425613699. Email: rasphys2@gmail.com

References:

- [1]. Y. S. Tang, S. F. Hu, C. C. Lin, N. C. Bagkar and R. S. Liu, *Appl. Phys. Lett.*, 2007, **90**, 151108.
- [2]. T. Nishida, T. Ban, and N. Kobayashi, *Appl. Phys. Lett.*, 2003, **82**, 3817.
- [3]. Y. Shimizu, K. Sakano, Y. Noguchi, and T. Moriguchi, *U.S. Patent*, 1999 5,998,925.
- [4]. (a) R. Grasser, A. Scharmann and K. R. Strack, *J. Lumin.*, 1982, **27**, 263.
 (b) A. M. Kaczmarek and R. Van Deun, *Chem. Soc. Rev.*, 2013, **42**, 8835.
 (c) S. H. Huang, D. Wang, C. X. Li, L. Z. Wang, X. Zhang, Y. Wan and P. P. Yang, *CrystEngComm*, 2012, **14**, 2235.
 (d) L. S. Cavalcante, F. M. C. Batista, M. A. P. Almeida, A. C. Rabelo, C. Nogueira, N. C. Batista, J. A. Varela, M. R. M. C. Santos, E. Longo, M. S. Li, *RSC Adv.*, 2012, **2**, 6438.
 (e) Y. Zhou and B. Yan, *CrystEngComm.*, 2013, **15**, 5694.
 (f) A. M. Kaczmarek, Y. Y. Liu, P. Van Der Voort and R. V. Deun, *Dalton Trans.*, 2013, **42**, 5471.
 (g) Maheshwary, B. P. Singh, J. Singh and R. A. Singh, *RSC Adv.*, 2014, **4**, 32605.
 (h) C. L. Li, C. K. Lin, X. M. Liu and J. Lin, *J. Nanosci. Nanotechnol.*, 2008, **8**, 1183.
- [5]. M. Nikl, P. Bohacek, N. Mihokova, N. Solovieva, A. Vedda, M. Martini, G.P. Pazzi, P. Fabeni, M. Kobayashi, M. Ishii, *J. Appl. Phys.*, 2002, **91**, 5041.
- [6]. M. Nikl, P. Bohacek, E. Mihokova, M. Kobayashi, M. Ishii, Y. Usuki, V. Babin, A. Stolovich, S. Zazubovich, M. Bacci, *J. Lumin.*, 2000, **87-89**, 1136.
- [7]. M. Nikl, *Phys. Status Solidi*, 2000, **178**, 595.
- [8]. X. Lou and D. Chen, *Mater. Lett.*, 2008, **62**, 1681.
- [9]. S. Shi, J. Gao, J. Zhou, *Opt. Mater.*, 2008, **30**, 1616.
- [10]. Z. Hou, C. Li, J. Yang, H. Lian, P. Yang, R. Chai, Z. Cheng and J. Lin *J. Mater. Chem.*, 2009, **19**, 2737.
- [11]. S. Basu, B. S. Naidu, B. Viswanadh, V. Sudarsan, S. N. Jha, D. Bhattacharyya and R. K. Vatsa, *RSC Adv.*, 2014, **4**, 15606.
- [12]. (a) B. Grobelna, M. Szabelski, K. Kledzik, A. M. Klunkowski, *J. Non-Cryst. Solids*, 2007, **353**, 2861.
 (b) S. Tsao, Y. P. Fu, C. T. Hu, *J. Alloys Compd.*, 2006, **419**, 197.
 (c) Q. Zhang, J. Wang, M. Zhang, W. Ding, Q. Su, *J. Rare Earths*, 2006, **24**, 392.
 (d) Y. Cao, Z. Zhao, J. Yi, C. Ma, D. Zhou, R. Wang, C. Li, J. Qiu, *J. Alloys Compd.*, 2013, **554**, 12.
- [13]. Z. Xia and D. Chen, *J. Am. Ceram. Soc.*, 2010, **93**, 1397.
- [14]. H. Qian, H.; J. Zhang and L. Yin, *RSC Adv.*, 2013, **3**, 9029-9034.
- [15]. B. F. Lei, B. Li, H. R. Zhang and W. L. Li, *Opt. Mater.*, 2007, **29**, 1491-1494.
- [16]. 16 F. Yang, Z. Yang, Q. Yu, Y. Liu, X. Li and F. Lu, *Spectrochim. Acta A.*, 2013, **105**, 626-631.
- [17]. H. M. Yang, Z. L. Wang, M. L. Gong and H. B. Liang, *J. Alloys Compd.*, 2009, **488**, 331.
- [18]. 18 Y. Tian, Y. Liu, R. Hua, L. Na and B. Chen, *Mater. Res. Bull.*, 2012, **47**, 59.
- [19]. T. Suhasini, J. S. Kumar, T. Sasikala, K. Jang, H. S. Lee, M. Jayasimhadri, J. H. Jeong, S. S. Yi and L. R. Moorthy, *Opt. Mater.*, 2009, **31**, 1167.
- [20]. L. Hu, H. Song, G. Pan, B. Yan, R. Qin, Q. Dai, L. Fan, S. Li, and X. Bai, *J. Lumines.*, 2007, **127**, 371.
- [21]. R. B. Podes and S. J. Dhoble, *Phys. Status Solidi B*, 1997, **203**, 571.
- [22]. H. Wu, Y. Hu, F. Kang, N. Li, G. Ju, Z. Mu, and Z. Yang, *J. Am. Ceram. Soc.*, 2012, **95**, 3214.
- [23]. Y. Zorenko, M. Pashkovsky, A. Voloshinovskii, B. Kuklinski and M. Grinberg, *J. Lumines.*, 2006, **116**, 43.
- [24]. Q. Xiao, Q. Zhou and M. Li, *J. Lumines.*, 2010, **130**, 1092.
 Y. Su, L. Li and G. Li, *Chem. Mater.*, 2008, **20**, 6060.
- [25]. W. Zhang, J. Long, A. Fan and J. Li, *Mater. Res. Bull.*, 2012, **47**, 3479.
- [26]. W. Wang, W. Pan, Y. Dai, S. Gai and P. Yang, *Optoelectronics and Advanced Materials – Rapid Communications.*, 2010, **4**, 1078.
- [27]. M. R. Krames, O. B. Shchekin, R. Mueller-Mach, G. O. Mueller, L. Zhou, G. Harbers and M. G. Craford, *J. Disp. Techn.*, 2007, **3**, 160-175.
- [28]. R. D. Shanon, *Acta Crystallogr., Sect. A: Cryst. Phys., Diffraction, Theor. Gen. Crystallogr.*, 1976, **32**, 751.
- [29]. S. Phokha, S. Pinitsoontorn, P. Chirawatkul, Y. Poo-arporn and S. Maensiri, *Nanoscale Res. Lett.*, 2012, **7**, 425.
- [30]. A. Kar and A. Patra, *Nanoscale*, 2012, **4**, 3608.
- [31]. M. Yin, A. Willis, F. Redl, N.J. Turro and S.P. O'Brien, *J. Mater. Res.*, 2004, **19**, 1208.
- [32]. V. Rothová, M. Svobodab, J. Buršík, Hradec nad Moravicí. (METAL) 2009, **5**, 19.
- [33]. I. Kaur, W. Gust, L. Kozma, Handbook of grain boundary and interface diffusion data (2nd edition) vol 1 Ziegler Press, Stuttgart (1989).
- [34]. A. K. Parchur, A. I. Prasad, S. B. Rai, R. Tewari, R. K. Sahu, G. S. Okram, R. A. Singh and R. Singh Ningthoujam, *AIP Advances*, 2012, **2**, 032119.
- [35]. S. Dutta, S. Som and S. K. Sharma, *Dalton Trans.*, 2013, **42**, 9654.
- [36]. L. Robindro Singh, R. S. Ningthoujam, V. Sudarsan, Iti Srivastava, S. Dorendrajit Singh, G. K. Dey and S. K. Kulshreshtha, *Nanotechnology*, 2008, **19**, 055201.
- [37]. B. P. Singh, A. K. Parchur, R. S. Ningthoujam, A. A. Ansari, P. Singh and S. B. Rai, *Dalton Trans.*, 2014, **43**, 4770.
- [38]. (a) M. Nicol and J. F. Durana, *J. Chem. Phys.*, 1971, **54**, 1436.
 (b) Z. C. Ling, H. R. Xia, D. G. Ran, F. Q. Liu, S. Q. Sun, J. D. Fan, H. J. Zhang, J. Y. Wang and L. L. Yu, *Chem. Phys. Lett.*, 2006, **426**, 85.
 (c) Y. B. Mao and S. S. Wong, *J. Am. Chem. Soc.*, 2004, **126**, 15245.
- [39]. A. P. de Moura, R. C. Lima, M. L. Moreira, D. P. Volanti, J. W. M. Espinosa, M. O. Orlandi, P. S. Pizani, J. A. Varela and E. Longo, *Solid State Ionics*, 2010, **181**, 775.
- [40]. S. P. S. Porto and J. F. Scott, *Phys. Rev.*, 1967, **157**, 716.

- [41]. P.F.S. Pereira, A.P. de Moura, I.C. Nogueira, M.V.S. Lima, E. Longo, P.C. de Sousa Filho, O.A. Serra, E.J. Nassar and I. L.V. Rosa, *J. Alloys Compds.*, 2012, **526**, 11.
- [42]. I. L. V. Rosa, A. P. A. Marques, M. T. S. Tanaka, F. V. Motta, J. A. Varela, E. R. Leite and E. Longo, *J. Fluoresc.*, 2009, **19**, 495.
- [43]. Y. Su, G. Li, Y. Xue and L. Li, *J. Phys. Chem. C.*, 2007, **111**, 6684.
- [44]. V. V. Atuchin, E. N. Galashov, O. Y. Khyzhun, A. S. Kozhukhov, L. D. Pokrovsky and V. N. Shlegel, *Cryst. Growth Des.*, 2011, **11**, 2479.
- [45]. A. Mukherjee, S. Basu, P. K. Manna, S. M. Yusuf and M. Pal, *J. Mater. Chem. C.* 2014, **2**, 5885.
- [46]. D. L. Wood and J. Tauc, *Phys. Rev. B.*, 1972, **5**, 3144.
- [47]. M. A. M. A. Maurera, A. G. Souza, L. E. B. Soledade, F. M. Pontes, E. Longo, E. R. Leite and J. A. Varela, *Mater. Lett.*, 2004, **58**, 727.
- [48]. D. P. Volanti, I. L.V. Rosa, E. C. Paris, C. A. Paskocimas, P. S. Pizani, J. A. Varela and E. Longo, *Opt. Mater.*, 2009, **31**, 995.
- [49]. B. Lei, Y. Liu, G. Tang, Z. Ye and C. Shi, *Mater. Chem. Phys.*, **2004**, 87, 227-232.
- [50]. A. K. Parchur, A. I. Prasad, A. A. Ansari, S. B. Rai and R. S. Ningthoujam, *Dalton Trans.*, 2012, **41**, 11032.
- [51]. D. L. Dexter, *J. Chem. Phys.*, 1953, **21**, 836.
- [53]. (a) A. K. Parchur, A. A. Ansari, B. P. Singh, T. N. Hasan, N. A. Syed, S. B. Rai and R. S. Ningthoujam, *Integr. Biol.*, 2014, **6**, 53.
(b) N. S. Singh, R. S. Ningthoujam, M. N. Luwang, S. D. Singh and R. K. Vatsa, *Chem. Phys. Lett.*, 2009, **480**, 237.
- [54]. D. L. Dexter and J. H. Schulman, *J. Chem. Phys.*, 1954, **22**, 1063.
- [55]. G. Blasse, *J. Solid State Chem.*, 1986, **62**, 207.
- [56]. G. Blasse, *Phys. Lett.*, 1968, **28**, 444.
- [57]. P. Li, Z. Wang, Z. Yang, Q. Guo, and X. Li, *Mater. Lett.*, 2009, **63**, 751.
- [58]. L.G. Van Uitert, *J. Electrochem. Soc.*, 1967, **114**, 1048.
- [59]. Y. Tian, B. J. Chen, R. N. Hua, H. Y. Zhong, L. H. Cheng, J. S. Sun, W. L. Lu, J. Wan, *Phys. B: Condens. Matter*, 2009, **404**, 3598.
- [60]. L. Wang, Q. Wang, X. Xu, J. Li, L. Gao, W. Kang, J. Shi and J. Wang, *J. Mater. Chem., C*, 2013, **1**, 8033.
- [61]. Y. He, M. Zhao, Y. Song, G. Zhao and X. Ai, *J. Lumin.*, 2011, **131**, 1144.
- [62]. B. P. Singh, A. K. Parchur, R. S. Ningthoujam, A. A. Ansari, P. Singh and S. B. Rai, *Dalton Trans.*, 2014, **43**, 4779.
- [63]. D. P. Dutta, R. S. Ningthoujam, and A. K. Tyagi, *AIP Advances*, 2012, **2**, 042184.
- [64]. V. Kumar, A. F. Khan and S. Chawla, *J. Phys. D: Appl. Phys.*, 2013, **46**, 365101.

† Electronic Supplementary Information (ESI) available: See DOI: 10.1039/b000000x/